Hindawi
Advances in Materials Science and Engineering
Volume 2019, Article ID 9654819, 15 pages
https://doi.org/10.1155/2019/9654819

Research Article

Detection Technology of Foamed Mixture Lightweight Soil Embankment Based on Ultrasonic Wave Transmission Method

Shikun Pu,[1,2,3,4] Baoning Hong,[1,2,3] Xin Liu ,[1,2,5] Fenqiang Xu,[6] and Hao Shan[1,2,3]

[1]*Key Laboratory of Ministry of Education for Geomechanics and Embankment Engineering, Hohai University, Nanjing 210098, China*
[2]*Jiangsu Research Center for Geotechnical Engineering Technology, Hohai University, Nanjing 210098, China*
[3]*Geotechnical Research Institute, Hohai University, Nanjing 210098, China*
[4]*Army Engineering University of PLA, Nanjing 210007, China*
[5]*Research Institute of Tunnel and Underground Engineering, Hohai University, Nanjing 210098, China*
[6]*Architectural Engineering Institute, Nanjing Institute of Technology, Nanjing 211167, China*

Correspondence should be addressed to Xin Liu; liuxin100@hhu.edu.cn

Received 8 December 2018; Revised 11 March 2019; Accepted 31 March 2019; Published 24 April 2019

Academic Editor: Ali Nazari

This study attempted to establish a process that uses the ultrasonic wave transmission method to correlate the ultrasonic parameters with the material properties of Foamed Mixture Lightweight Soil (FMLS). The results were then applied for the defect detection of the FMLS embankment. First, the ultrasonic wave velocity (UPV) and amplitude (UPA) of FMLS with different mix proportions were collected continuously from 3rd day to 45th day in the curing age. The relationships between UPV versus FMLS elastic modulus, unconfined compressive strength, and density were calibrated. The variations in the ultrasonic parameters owing to the test distance and crack width were recorded. Then, the laboratory tests were reproduced through numerical simulation approach. Finally, the reliability and accuracy of the proposed detection method for FMLS were proved and validated through on-site tests. The proposed methodology, which is simple, stable, and reliable, was found to be suitable for the quality diagnosis of FMLS embankments after construction and during operation.

1. Introduction

Foamed mixture lightweight soil (FMLS), a new type of geotechnical material, has now been used in highway embankment filling (Figure 1) and widening, landslide treatment, and tunnel filling because of its lightweight and excellent mechanical properties [1]. Different from traditional embankment fillers, the performance of FMLS degrades with time and environment changes [2]. Finding a method to detect the defectiveness of FMLS embankments to minimize the damage to highway pavements and embankments is a crucial problem when using this material as an embankment filler.

The state-of-art embankment testing apparatuses, such as the nuclear density gauge [3] and falling weight deflectometer [4], focus on the compactness of the embankment. Although these techniques are standard for soil embankment testing, they have not been sufficiently studied regarding their suitability for FMLS embankments.

The ultrasonic wave transmission method, as a type of nondestructive testing technology, has many successful applications in infrastructure quality inspections, including the integrity testing of cast-in-place piles [5], strength testing of concrete, and crack detection in concrete. Research findings on the relationships between the ultrasonic parameters and concrete quality are abundant. Many countries have established ultrasonic wave transmission detection standards [6–10].

Since the 1970s, researchers have been using the ultrasonic wave transmission method to determine the relationship between the ultrasonic parameters and elastic modulus of cement mortar [11]. Subsequently, this method

Figure 1: Foamed mixture lightweight soil as highway embankment filler.

was found to be suitable for studying the hydration of cement paste in the oil industry [12, 13]. Previous studies indicated that a high solid concentration causes less wave attenuation [14]. Besides, the bubble content [15], moisture content, porosity, and permeability [16] are essential factors that are attenuating the ultrasonic parameters. According to, the quality of a cement paste or a cement block can be well estimated by using the measured velocity and amplitude of the ultrasonic wave [17]. In some conditions, the precalibration is necessary for using ultrasonic wave velocity (UPV) to estimate the compressive strength f_c [18].

An ultrasonic wave has also been used to study the properties of cement with different admixtures such as asphalt cement [19], fly ash cement [20], and foamed cement. Davraz measured the relationship between the UPV and the thermal conductivity of foamed cement [21]. SheWei used an ultrasonic pulse to examine the solidification behavior of foamed cement. He also presented the relationship between the ultrasound parameters and its setting time [22].

In fact, short-term to long-term performances of concrete have been sufficiently studied using the ultrasonic wave transmission method. A previous study of cement properties using this method focused on the relationship between the setting behavior and UPV. FMLS is a cement-based porous material that is loose and has a strength of less than 2 MPa. Nowadays, FMLS is widely used as embankment fill. However, the applications of ultrasonic wave transmission for studying its physical and mechanical properties of the FMLS have not been found in practice. Concurrently, it is also necessary to verify the reliability of the waveforms by using a calibration curve for the on-site tests [23].

This study uses the ultrasonic wave transmission method to detect the UPV and UPA of an FMLS with different mix proportions and calibrates the variation curves between the material and ultrasonic parameters. The finite element method will be used to simulate the propagation of the ultrasonic pulse wave in the FMLS to reproduce the laboratory test results. Finally, based on the calibration and simulation, a quality diagnosis of an embankment will be performed in the on-site test.

2. Laboratory Test

2.1. Materials and Apparatuses. Cement is the primary raw material for preparing FMLS. Because both the density and strength of FMLS are very low, there is a strict requirement of cement quality during the preparation. Portland cement manufactured by Nanjing ZhongLian Cement Co., Ltd., is used in the laboratory test. The compressive strength of the tested Portland cement is 42.5 MPa at 28 days, and its specification details presented in Table 1. The ultrasonic wave detecting apparatus is a ZBL-510 nonmetallic ultrasonic detector manufactured by Beijing ZBL Science & Technology Co., Ltd. The frequency of the transducer is 25 kHz, and the transducer voltage is 500 V.

2.2. Mix Proportions. At present, there is no standardized regulation for the proportioning of FMLS. Two Chinese standards, CECS249 [24] and CJJ/T177 [25], were adopted for selecting the mixing proportions. CJJ/T177 states that when the strength of the FMLS increases from 0.5 MPa to 1.0 MPa with the step of 0.1 MPa, the cement content increases by 25 kg, water increases by 10 kg, and foam decreases by 15.5 L (a reduction of 18.1 L between 0.6 MPa and 0.5 MPa) (Table 2). This study will use the mix proportions listed in Table 3, which meet the requirements of the specifications also reflect the fluctuations in the ultrasonic parameters caused by the changes in the materials.

2.3. Sample Preparation. The process of preparing the FMLS in the laboratory is listed as follows:

(a) Materials are weighed according to Table 3

(b) Water (minus the weight of the foam) is added to the mixture, with mixing for 5 min

(c) The foam is weighed and mixed with cement paste until the foam is dispersed

(d) Transparent plastic plates with thicknesses of 0.1 mm, 0.2 mm, and 0.3 mm are submerged into the cement slurry and taken out after the initial setting to form initial cracks with different widths

(e) The paste is placed into a mold, which is removed after two days

2.4. Test Scheme. Six samples with different mix proportions were prepared based on the above process. Each sample was cast in three sizes: $100 \times 100 \times 100$ mm, $100 \times 100 \times 200$ mm, and $100 \times 100 \times 300$ mm (Figure 2). Cubes with initial crack widths of 0.1 mm, 0.2 mm, and 0.3 mm were also prepared. The UPV and UPA will be measured and studied by considering the corresponding measuring distances and crack widths for analyzing the relationship between them and establishing the quality inspection system. A testing example is shown in Figure 3.

Table 1: Performances of cement used in the laboratory test.

No.	Index		Compulsory requirement	Measured results
1	Specific surface area (m^2/kg)		≥400	348
2	Water requirement of normal consistency (%)		—	28.8
3	Stability		Boiling method qualified	Qualified
4	Setting time (min)	Initial	≤55	40
		Final	≤590	300
5	Flexural strength (MPa)	3 days	≥3.5	4.8
		28 days	≥6.5	8.7
6	Compressive strength (MPa)	3 days	≥17.0	23.4
		28 days	≥42.5	49.5

Table 2: Proposed mix proportions by CJJ/T177.

Designed strength (MPa)	Consumption per cubic meter		
	Cement (kg)	Water (kg)	Bubble (L)
0.50	275	190	721.3
0.60	300	200	703.2
0.80	350	215	672.1
1.00	400	230	641.0

Table 3: Mix proportions of laboratory test.

No.	Consumption per cubic meter			WCR
	Cement (kg)	Water (kg)	Bubble (L)	
1	300	200	703.2	0.67
2	350	215	672.1	0.61
3	400	230	641.0	0.58
4	425	237.5	625.5	0.56
5	475	252.5	594.4	0.53
6	525	267.5	563.3	0.51

(a) (b)

Figure 2: FMLS samples: (a) paste in curing; (b) form removal.

3. Analysis of Laboratory Results

3.1. Correlation between Curing Period and Ultrasonic Parameters. The variation in the UPV and UPA of the FMLS cube samples under natural curing is shown in Figures 4 and 5, and their rate curves are displayed in Figures 6 and 7. It is observed that the UPV curves of all samples increase, but the rate of the UPV decreases with the curing age. At 45 days, all UPVs are between 1.0 and 1.5 km/s; these values are much lower than the UPV of concrete [26] and close to that of rigid closed-cell plastic foams [27]. The results also show a favorable negative correlation between the water-to-cement ratio (WCR) and UPV. The UPV increases when the WCR decreases.

Although the trend of UPA is similar to that of the UPV, there are still some differences between their curves. First,

Figure 3: UPV test on 100 mm sample.

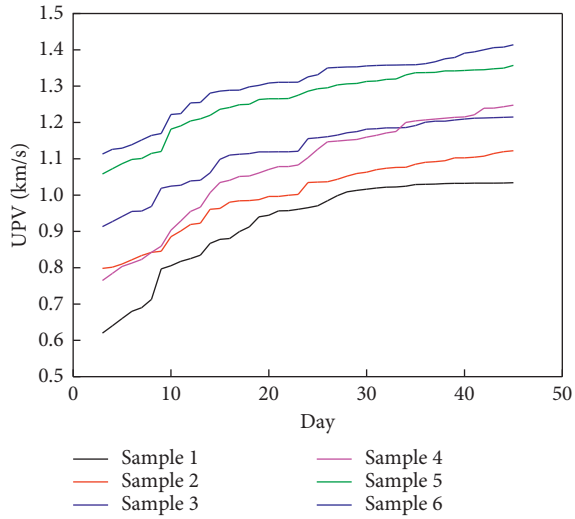

Figure 4: UPV versus curing period for FMLS.

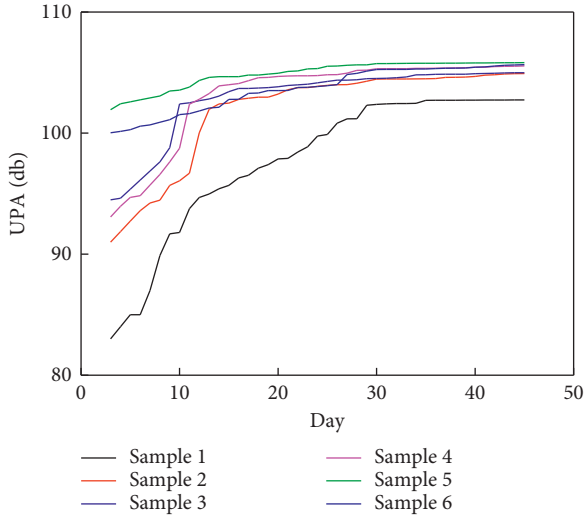

Figure 5: UPA versus curing period for FMLS.

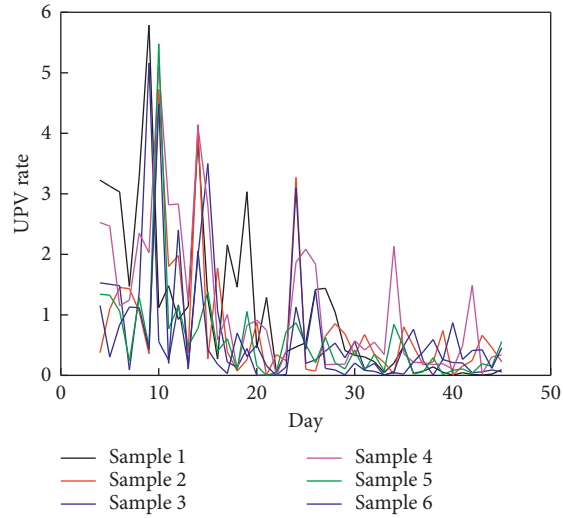

Figure 6: UPV rate versus curing period for FMLS.

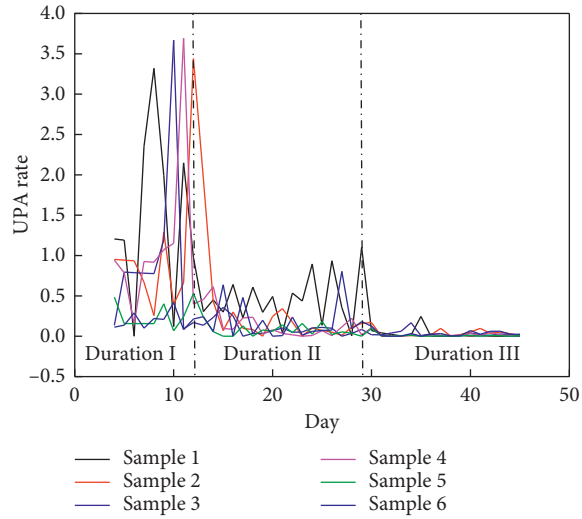

Figure 7: UPA rate versus curing period for FMLS.

the UPA rate decreases to less than 1% in about 16 days, whereas the UPV rate decreases to this level after more than 28 days. Second, the differences in the UPAs are not as obvious as those in the UPVs. Third, the UPA rate shows three characteristic durations, from 3 to 12 days, from 13 to 29 days, and after 30 days. However, the UPV rate did not exhibit such a feature.

SheWei measured the UPV of a foamed concrete mixture within the first 50 h and found that the UPV curve exhibited an S-shape with three stages, and the UPV rate decreased from 70% to less than 10% [22]. In the present experiments, it can be observed that the UPV of the FMLS continues to increase after 72 hours. But the change rate, whose maximum is 6%, is much lower than the results presented by SheWei. Rao and Gunasekaran examined the long-term trends of the UPV in roller-compacted concrete

[20] and coconut-shell concrete [28]. For all those tested concrete types, the UPV increased between 0 and 28 days and tended to stabilize after 28 days. These patterns were similar to the findings of present experiment with respect to FMLS.

3.2. Correlation between UPV and Strength/Density/Modulus of Elasticity. The density, Poisson's ratio, unconfined compressive strength, etc., are calibrated by geotechnical experiments. In general, the relationship between the UPV of solids and their elastic modulus is [29]

$$E_{\mathrm{d}} = \frac{c_L^2 \rho (1+\mu)(1-2\mu)}{(1-\mu)}, \quad (1)$$

where E_{d} is the elastic modulus (MPa), c_{L} is the UPV (km/s), ρ is the density (kg/m^3), and μ is Poisson's ratio.

Substituting c_{L}, ρ, and μ in equation (1), the elastic moduli of the samples can be calculated correspondingly. All of the ultrasonic and material parameters are listed in Table 4.

The calibration curves of the unconfined compressive strengths, densities, elastic moduli, and UPVs are displayed in Figure 8. It can be observed that the elastic modulus and unconfined compressive strength of the FMLS have exponent relations to the UPV. A linear function obtained from the linear regression approach is applied to describe the relationship between density and UPV.

$$E_{\mathrm{d}} = -310.27 + 76.97 \cdot e^{2.13 \cdot v}, \quad (2)$$

$$S = -0.25297 + 0.15368 \cdot e^{1.7357 \cdot v}, \quad (3)$$

$$\rho = -354.94 + 690.08 \cdot v, \quad (4)$$

where E_{d} is the elastic modulus (MPa), S is the unconfined compressive strength (MPa), ρ is the density (kg/m^3), and v is the UPV (km/s).

3.3. Correlation between Measuring Distance and Ultrasonic Parameters. Ultrasonic signals attenuate rapidly in porous solids. If the distance between measuring points is too long, the received signal will become weak (or even zero) and heavily distorted. If the measuring points are too close to each other, the size effect owing to the decrease in the distance between measuring points will cause the detected value to fluctuate. Hence, when the ultrasonic wave transmission method is used in a quality diagnosis of an FMLS embankment, the selection of the measuring distance is a key issue.

Three types of specimens with sizes of 100 mm, 200 mm, and 300 mm are prepared in the laboratory test, and specimens with sizes of 400 mm, 500 mm, and 600 mm are combinations of the 100 mm, 200 mm, and 300 mm specimens bonded with vaseline. Previous studies showed that the acoustic impedance of vaseline is basically the same as that of FMLS [30, 31], which is about 3 MRayl. When the couplant thickness is less than 0.5 mm, the influence of the couplant on the test results of cement-based materials can be neglected [32]. Therefore, vaseline can be used for bonding the samples with little influence on the transmission of sound waves.

The relationship between the measuring distance and the UPV variation is presented in Figure 9. The UPV is stable when the measuring distance is from 100 to 300 mm, and it begins to decrease when the measuring distance longer than 400 mm. Compared with the UPV, the UPA decreases in a steeper slope with respect to the measuring distance (Figure 10). The maximum attenuation under different measuring distances that can be detected is 60.9%, and this occurs in the 500 mm sample (Sample 1). Once the measuring distance reaches 600 mm, the signal of Sample 1 cannot be detected, and those of the others become unstable. In a previous study, Jones reported on the maximum test measuring distance of concrete at different frequencies [33]. He believed that the test measuring distance of concrete should be between 200 and 1500 mm when the natural frequency of the transducer is between 20 kHz–40 kHz. Based on the results of the present experiment, it is suggested that the maximum measuring distance for the defect detecting of FMLS should be less than 500 mm.

3.4. Correlation between Crack Width and Ultrasonic Parameters. FMLS is a brittle material with low strength, and it is easy to crack after loading. Thus, the detection of cracks is critical for the applications of FMLS. Although the precast crack is not precisely identical to the actual crack, the difference between the precast crack and the actual crack is subtle in the context of using the ultrasonic wave method for detecting the internal cracks. Figures 11 and 12 display the variation in the ultrasonic signals at different crack widths. Both the UPV and UPA decrease with an increase in the crack width. However, the attenuation of the ultrasonic parameters caused by the microdefects is less sensitive than the attenuation caused by the growth of the measuring distance. Despite the insignificant attenuation, ultrasonic waveform distortions caused by the cracks are observed. When the ultrasonic pulse passes through the crack vertically, the waveforms of the four specimens numbered as S1-C2, S2-C2, S4-C1, and S5-C2 (Figure 13) become abruptly attenuated. Since the waveform attenuation caused by microcracks, bubbles, and other factors can be successfully detected by using the nondestructive testing method for concrete [34], mortar [17], ceramics, and aluminum [35], the ultrasonic traveling wave distortion can also be used as an important indicator for the defect detection of FMLS.

4. Numerical Simulation

4.1. Simulation Scheme. To reproduce the laboratory results, ABAQUS is used to simulate the transmission features of the ultrasonic wave in the FMLS. An elastic model is used in the simulation, and the parameters of the material, such as the elastic moduli and densities, are listed in Table 4. Because of the unknown values of the pulse, a short displacement with a frequency of 25 kHz and amplitude of 10^{-9} [36] is applied at

Table 4: Ultrasonic and material parameters of the FMLS.

No.	Ultrasonic parameters	Material parameters			
	C_L (km/s)	E_d (MPa)	S (MPa)	ρ (kg/m^3)	Poisson's ratio μ
1	1.034	381.92	0.67	363.12	0.2013
2	1.122	526.85	0.81	417.57	0.1987
3	1.215	702.77	1.03	476.34	0.1976
4	1.248	796.88	1.12	512.71	0.1955
5	1.357	1054.27	1.30	571.95	0.1937
6	1.414	1252.50	1.57	629.88	0.1929

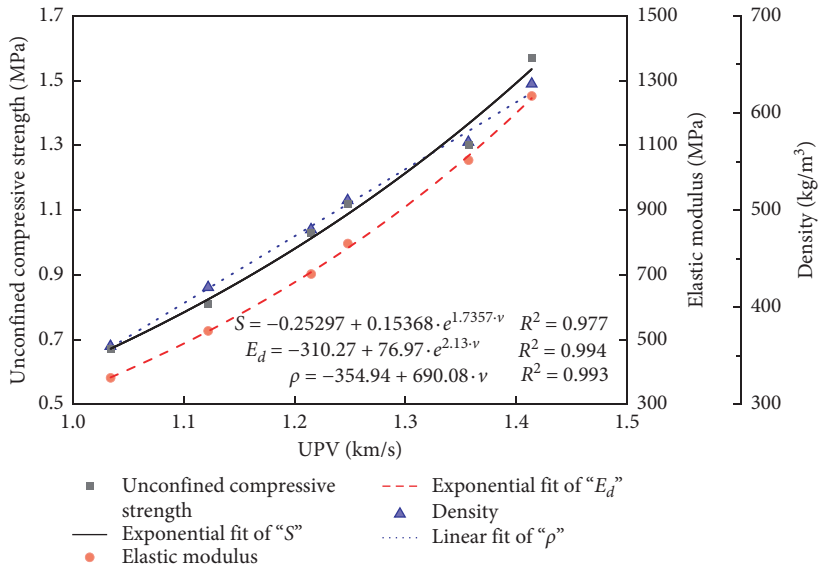

Figure 8: Unconfined compressive strength, density, and elastic modulus versus UPV.

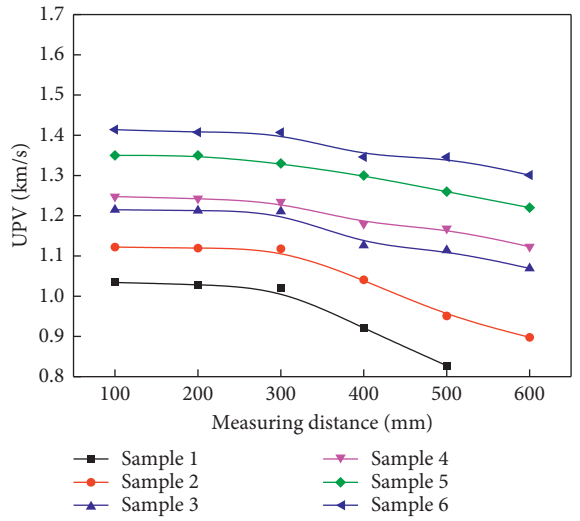

Figure 9: Variation of UPV with measuring distance.

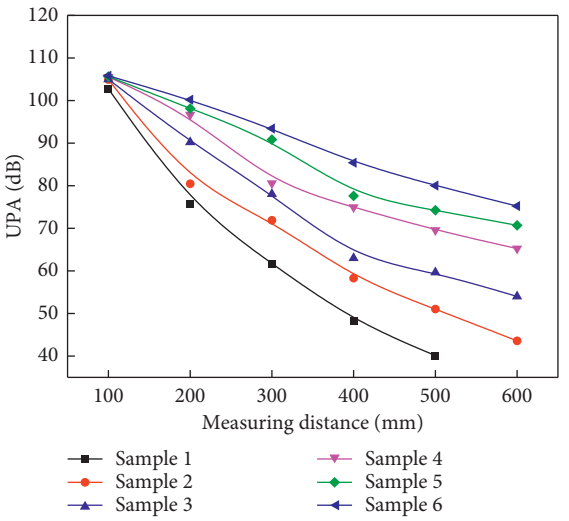

Figure 10: Variation of UPA with measuring distance.

the center of one side of the specimen to simulate the pulse emitted by a transducer. A receiver node is set at the center of the opposite side to collect the time of signals traveling from one side to the other (Figure 14). Although this method cannot accurately simulate all of the ultrasonic characteristics, it is still possible to qualitatively reproduce the laboratory tests using specified parameters.

The ultrasonic pulse wave velocity is computed by

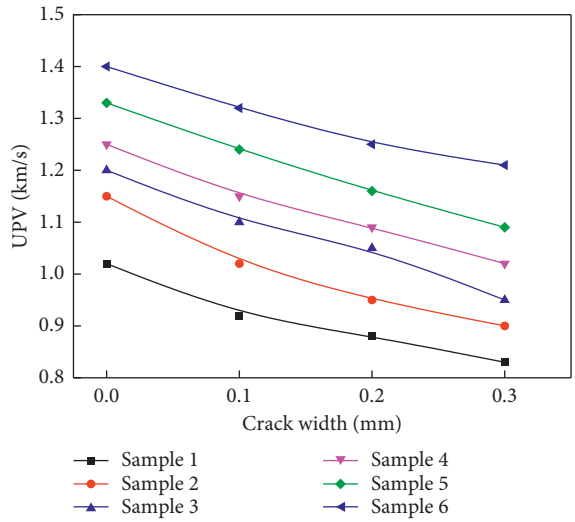

Figure 11: Variation of UPV with crack width.

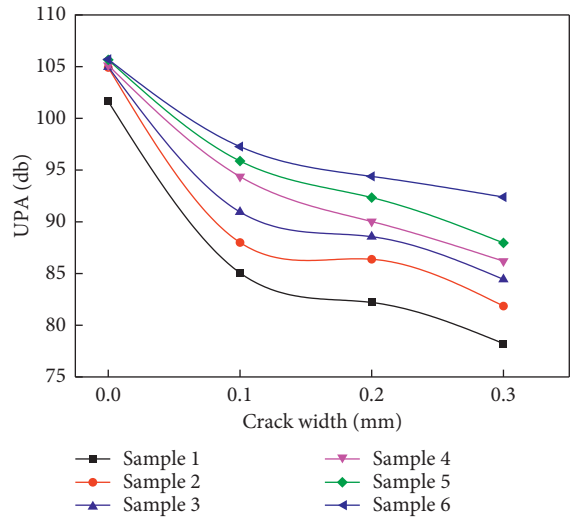

Figure 12: Variation of UPA with crack width.

$$v = \frac{L}{t}, \tag{5}$$

where v is the simulated UPV (km/s), L is the size of the simulated specimen (mm), and t is the transmitted time of the wave (s).

4.2. Determination of Head Wave. There have been many studies on the ultrasonic wave transmission method via finite element simulation [37–39]. The major focus of these studies was to determine the occurrence time and amplitude of the ultrasonic pulse head wave. Most of the studies [36, 40] used the moment when the displacement of the receiver node first reached the maximum (arrows in Figure 15) as the occurrence time of the head wave. In fact, the process of an ultrasonic wave passing through a specimen can be described as follows: First, the wave arrives at the position of the receiver node, and it stirs the receiver node. Then, the velocity of the node reaches its maximum. Finally, the displacement of the node reaches its maximum. Therefore, it will be more accurate to choose the moment when the velocity of the receiver node reaches the maximum (arrows in Figure 16) as the arrival time of the head wave.

In general, the displacement of the receiver node is often used to describe the UPA indirectly. This is reasonable but not suitable for studying the UPAs of different materials. The displacements of the receiver nodes of Samples 1 to 6 in Figure 15 decrease successively owing to the increase in the elastic modulus, which is contrary to the laboratory results (Figure 5). According to the acoustic emission theory, the acoustic wave emitted from a solid is strongly related to its strain energy, which is produced by the same deformation, and the strain energy depends on the elastic modulus [41]. A smaller water-to-cement ratio implies a high elastic modulus of the FMLS, which means a small attenuation of the ultrasonic pulse wave propagation and a large UPV and UPA. Figure 17 shows the strain energy at the receiver nodes of Samples 1 to 6. Compared with the trend of displacement, the trend of strain energy at the receiver node is more similar to the laboratory result.

4.3. Correlation between E_d, S, ρ, and UPV. The UPV is calculated using the moment when the velocity of the receiver node reaches its first maximum. Substituting this value in equations (2)–(4), the simulated E_d, S, and ρ can be calculated. The velocities calculated for the moments when the displacement and strain energy reach their first maximum are also substituted in equations (2)–(4), and the four types of velocities are plotted in Figure 18. Obviously, all of the simulated and calibrated E_d, S, and ρ values exhibit the same trend. The simulated values obtained from the UPV calculated using the time when the velocity of the receiver node first reaches the maximum are closer to the calibrated values.

4.4. Correlation between Measuring Distance and Ultrasonic Parameters. Figure 19 describes the relationship between the arrival time of the stress wave and measuring distance. As the measuring distance increases, the time required for the stress wave to reach the boundary surface becomes longer. However, the velocity calculated by equation (5) does not decrease obviously as that in the laboratory results (Figure 20). According to equation (1), the UPV of a solid only relates to its elastic modulus, density, and Poisson's ratio and is independent of the measuring distance. Therefore, without considering the dissipation and attenuation, the stress wave speed stays constant when the measuring distance increases. The attenuation of the simulated UPV is derived from the bulk viscosity, which affects the strain rate of the element [42]. According to the test results, the simulated wave velocity is not as significantly attenuated as the measured wave velocity with the growth of the measuring distance. In comparison, the strain energy has better performance when reflecting the measured amplitude attenuation.

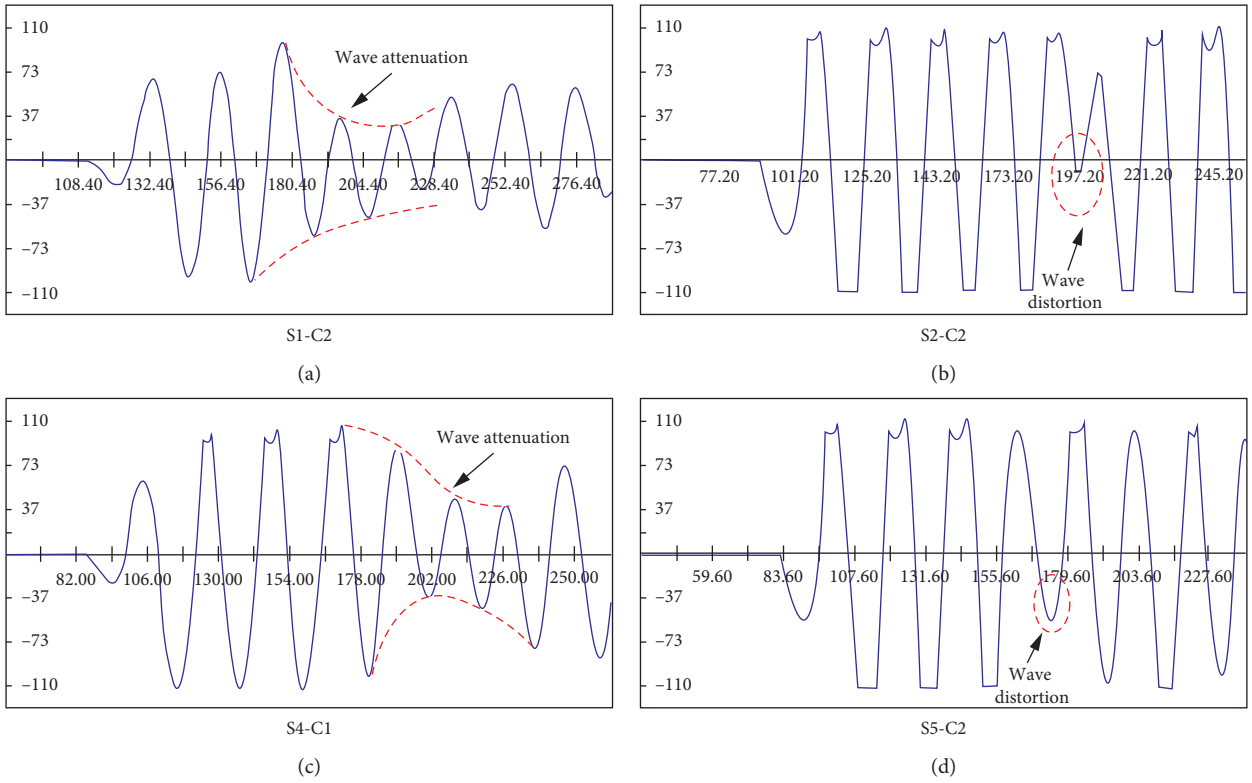

Figure 13: Waveform distortions. "S" is short for sample, and "C" is short for crack width. For example, "S4-C1" indicates result of sample 4 with crack width of 0.1 mm.

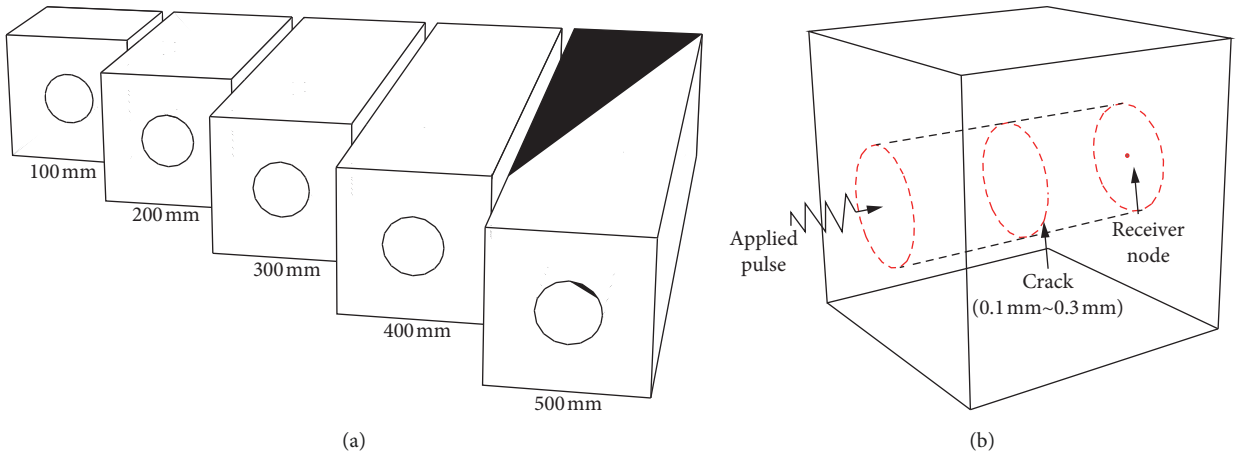

Figure 14: Simulation test blocks: (a) with different measuring distances; (b) with different crack widths.

The simulated strain energy changes with respect to the measuring distances are shown in Figure 21. The strain energy becomes more detectable with increasing E_d and ρ. Figure 21 also suggests that the measuring distance significantly affects the transmission of the ultrasonic wave. As the measuring distance becomes longer, the strain energy clearly decreases. Figure 21(a) shows that the peak of the strain energy can barely be detected in Sample 1 when the measuring distance reaches 500 mm, but it becomes clearer with the WCR decrease. The numerical simulation well reproduces the laboratory results, i.e., the maximum measuring distance should be less than 500 mm.

4.5. Correlation between Crack Width and Ultrasonic Parameters. Figures 22 and 23 depict the simulated wave velocity and strain energy as a function of the crack width. It can be observed from the simulation studies that the effect of the cracks on the wave velocity is minor, but it is significant with regard to the strain energy. The strain energies of all the

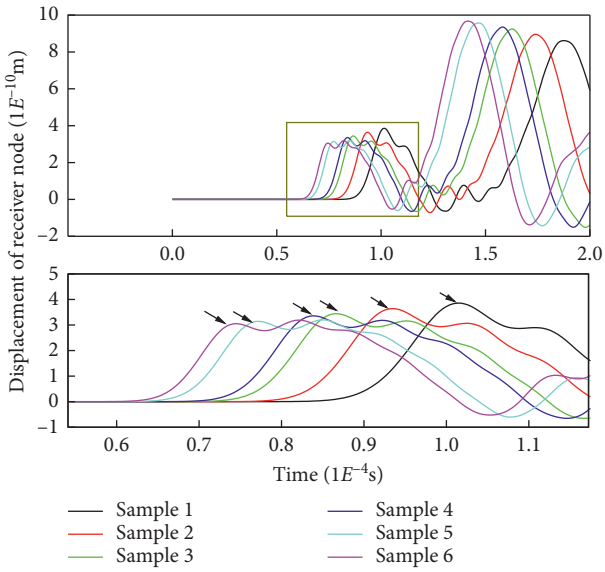

Figure 15: Displacement of receiver node.

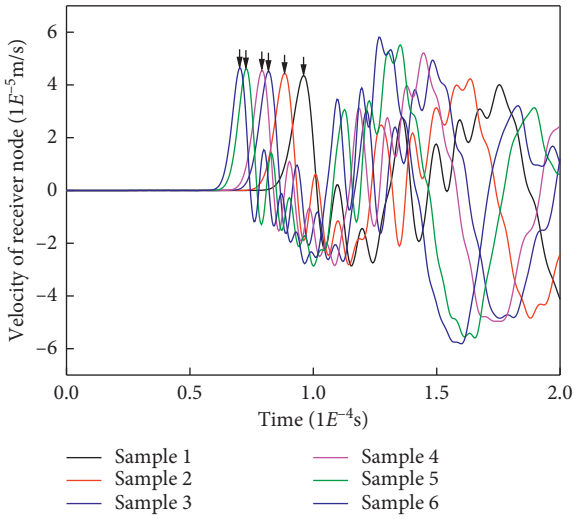

Figure 16: Velocity of receiver node.

defective samples decrease by 50% compared with the reference samples (without cracks). Although the simulated strain energy curves and measured UPA curves have similar shapes, their values are different. Thus, the strain energy can only be used as a qualitative reference for the UPA. The simulated waveform of Sample 6 is plotted in Figure 24. A clear difference in the waveform can be observed between the healthy and defective samples, but the waveform deviations in the different crack samples are difficult to differentiate. In fact, the strain energy of Sample 6 containing a 0.1 mm crack is only 1% higher than that of the case with a 0.3 mm crack. Hence, an increase in the crack width does not contribute significantly to the strain energy attenuation. This result is similar to the results from Roberts: the wave attenuation was less sensitive to the variations in the microcrack [43]. While reproducing the laboratory test results, the results of the numerical simulations illustrate the

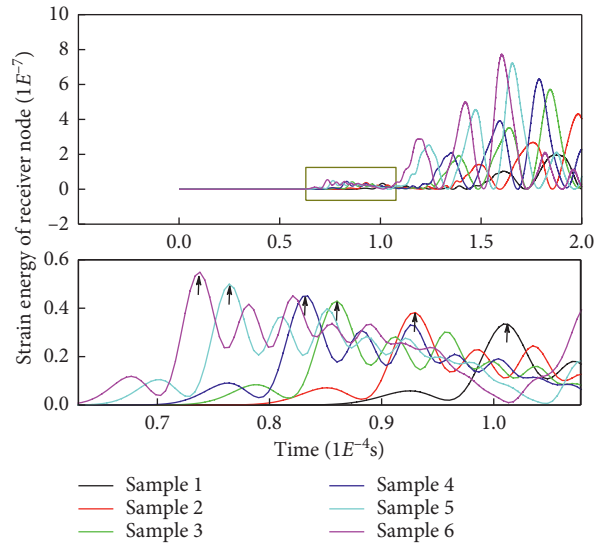

Figure 17: Strain energy of receiver node.

importance of the waveform distortion in FMLS microdefect detection from another perspective.

5. On-Site Test

5.1. Test Embankment. To verify the applicability of the ultrasonic wave transmission method for FMLS embankments in a nondestructive manner, an on-site test section with dimensions of $10\,m \times 9\,\text{m} \times 1.75\,\text{m}$ (length × width × depth) was set-up at a ramp in the Guangming highway (Figure 25). The mixing proportion of this target section was identical to that of Sample 2 listed in Table 3. The cross-hole loggings were drilled, and the access tubes were installed to obtain the propagation of the ultrasonic wave in the FMLS embankment (Figure 26).

5.2. Test Procedure. The plastic access tubes, which had a 50 mm diameter and 5.0 mm wall, were installed before casting the embankment. Each set of the cross-hole loggings had two access tubes, and the measuring distance between these tubes was 500 mm. Ten sets of access tubes at each side of the test section (20 tubes in total) were prepared. This configuration ensured that the test was performed without affecting the highway construction. After the highway was completed, these access tubes could still be used during its operation.

After the installation, the perpendicularity and sealing performance of each tube were examined. The top of each tube was covered to prevent foreign objects from falling into the tube and blocking the tubes during the embankment casting.

Nondestructive testing of the FMLS embankment was performed on 45th day after casting. Before the test, the performance of the equipment was checked, and the tubes were filled with water. A transmitter and receiver were dropped into the bottom of the tubes, and the positions of the two transducers were maintained at same horizontal level during the experiments. Both transducers were pulled

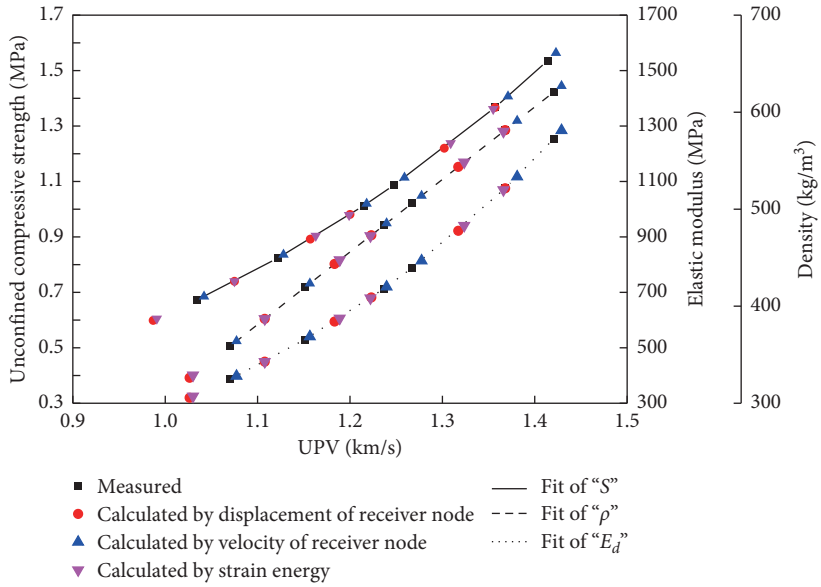

Figure 18: E_d, S, and ρ versus UPV (comparison between experimental results and simulation results).

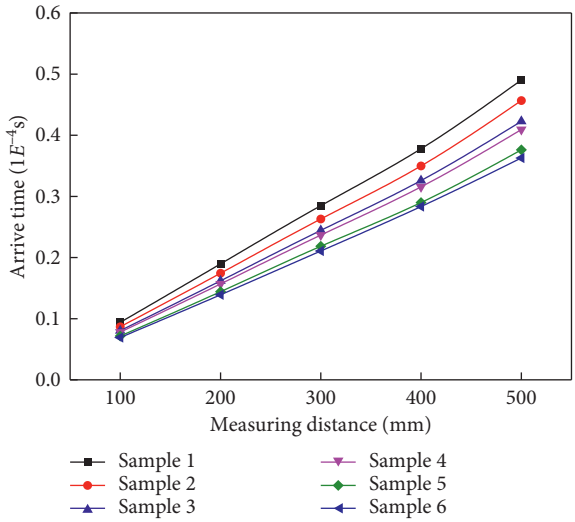

Figure 19: Arrival time versus measuring distance.

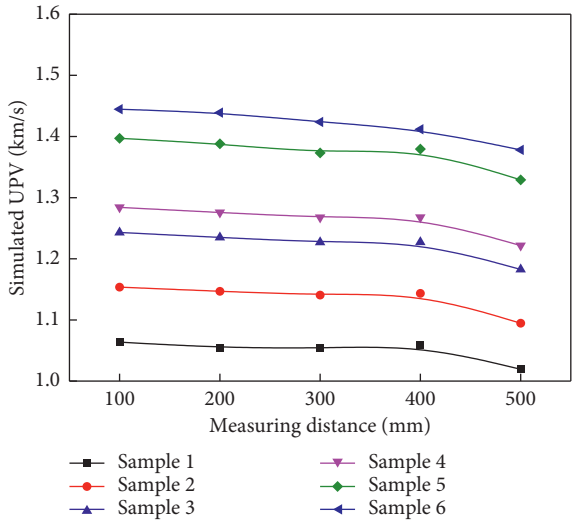

Figure 20: Simulated UPV versus measuring distance.

up synchronously, and the equipment started to record. The ultrasonic data were recorded each time the transducers were lifted by 200 mm. Each set of access tubes recorded 9 groups of data, and 90 ultrasonic parameters in total were collected (Figure 27).

5.3. Test Results. Figure 28 shows the results of the ultrasonic parameters obtained during the field test. According to Figure 28, the maximum UPV is 1.29 km/s, the minimum is 1.01 km/s, and the average is 1.14 km/s. By substituting the detected UPV into equations (2)–(4), the physical and mechanical parameters are estimated. All unconfined compressive strengths, elastic moduli, and densities are also plotted in Figure 28. The calculated maximum unconfined compressive strength is 1.19 MPa, the minimum is 0.63 MPa, and the average is 0.87 MPa. The maximum elastic modulus is 875.73 MPa, the minimum is 348.73 MPa, and the average is 568.64 MPa. The maximum density is 535.35 kg/m^3, the minimum is 341.11 kg/m^3, and the average is 432.45 kg/m^3. Although the results are discrete, they are all within 1.6 times of their standard deviations, which have a 95% guarantee. The probability distributions of the calculated parameters are as the same as those of the UPV. Moreover, the maximum amplitude detected is 78.2 dB, the minimum is 49.6 dB, and the average is 58.8 dB, which is higher than the amplitude of Sample 2 but less than that of Sample 4. No waveform anomalies are observed. Therefore, the test results infer that the unconfined compressive strength of the FMLS embankment is between 0.6 MPa and 1.2 MPa. The embankment is considered qualified if using "all the measured strength are greater than 75% of the design value" as the evaluation criteria [44].

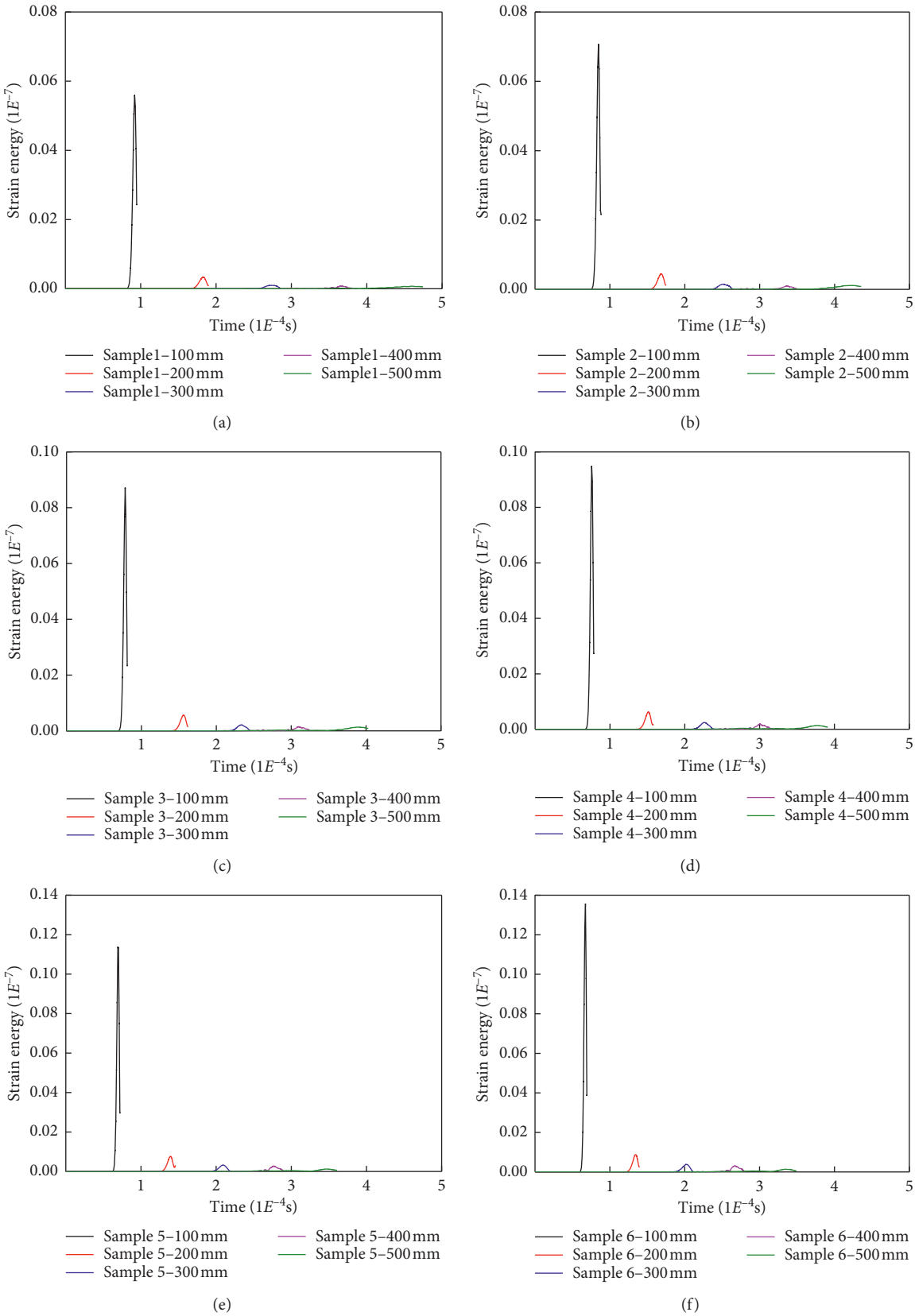

Figure 21: First appearance of strain energy: (a) Sample 1, (b) Sample 2, (c) Sample 3, (d) Sample 4, (e) Sample 5, and (f) Sample 6. When the measuring distance arrives at 500 mm, the strain energy peak of the sample 1 becomes difficult to notice.

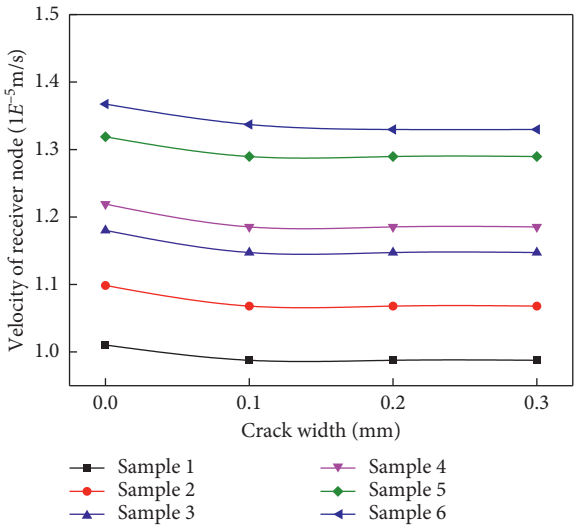

Figure 22: Velocity of receiver node versus crack width.

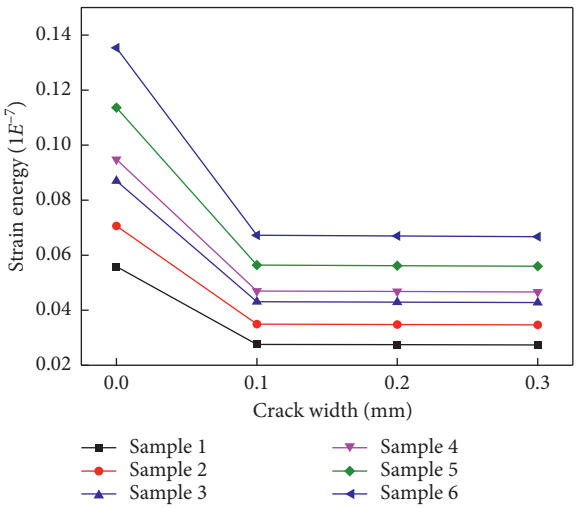

Figure 23: Strain energy of receiver node versus crack width.

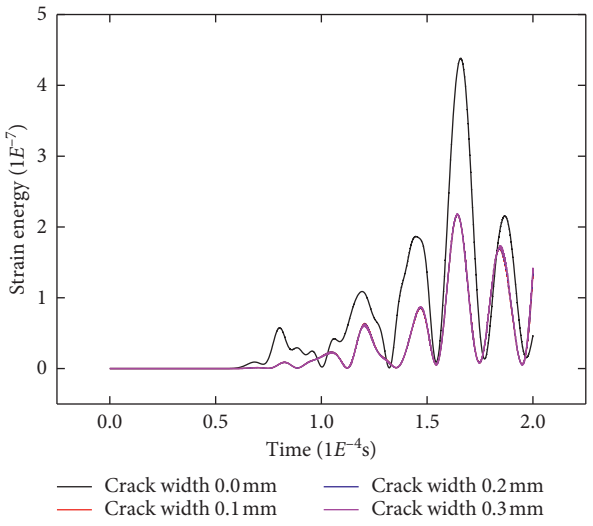

Figure 24: Strain energy of Sample 6.

Figure 25: Test site.

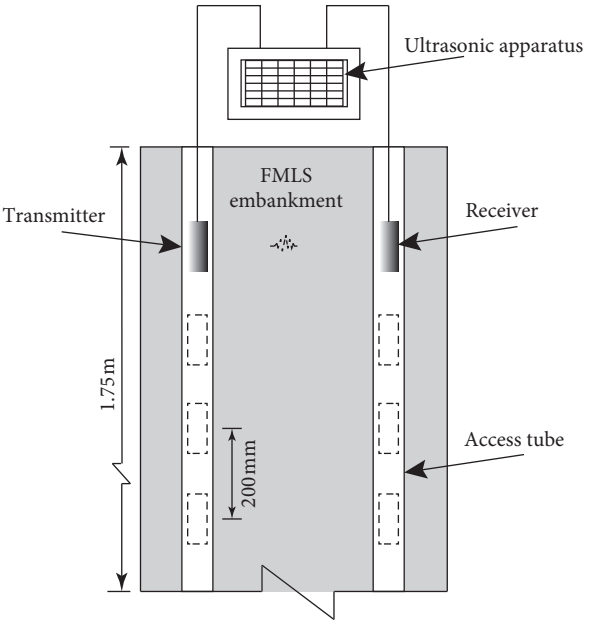

Figure 26: Cross-hole ultrasonic loggings in FMLS embankment.

6. Conclusion

In this paper, a procedure for detecting FMLS embankments using ultrasonic wave transmission was introduced. It was possible to obtain the basic material parameters of the embankment by linking the laboratory calibration curve with the on-site test results. Based on an analysis, the following conclusions were drawn:

(1) The time-varying physical property and the internal crack evolution in the FMLS embankment can be recorded and detected in the early stage by using the ultrasonic wave transmission method.

Figure 27: Ultrasonic parameter collection.

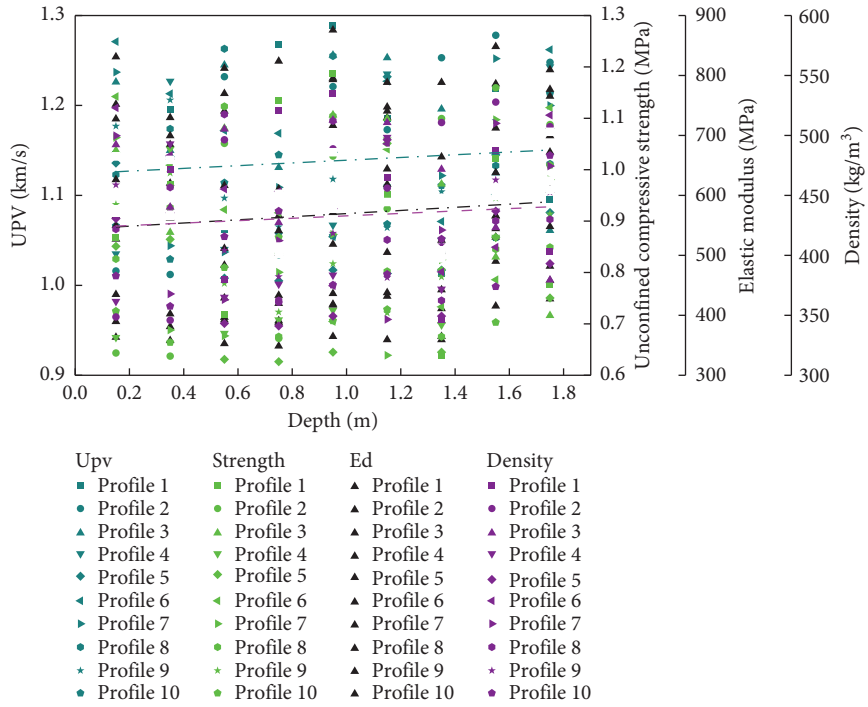

Figure 28: On-site test result. Dashed lines indicate linear fitting of UPV, strength E_d, and density.

(2) The ultrasonic wave parameters of the FMLS are correlated with the curing age. After the 30th day, the wave velocity and amplitude tend to be stable.

(3) The elastic modulus, strength, and density can be calibrated by the UPV. The proposed equations for the relationship between the UPV and the elastic modulus, strength, and density are given by $E_d = -310.27 + 76.97 \cdot e^{2.13 \cdot v}$, $S = -0.25297 + 0.15368 \cdot e^{1.7357 \cdot v}$, and $\rho = -354.94 + 690.08 \cdot v$.

(4) The attenuation of the UPA is more obvious than that of the UPV when the measuring distance increases. The maximum measuring distance for the detection of an FMLS should be less than 500 mm.

(5) Cracks affect not only the ultrasonic parameters but also the waveform. The distortion of the waveform deserves more attention when identifying defects in an FMLS.

Abbreviations and Variables

FMLS: Foamed Mixture Lightweight Soil
UPV: Ultrasonic wave velocity (km/s)
UPA: Ultrasonic wave amplitude (dB)
E_d: Elastic modulus (MPa)
S: Unconfined compressive strength (MPa)
ρ: Density (kg/m^3)

v: Ultrasonic pulse velocity (km/s)
L: Size of simulated block (mm)
t: Transmitted time of UPV (s).

Data Availability

The data used to support the findings of this study are included within the article.

Conflicts of Interest

The authors declare that they have no conflicts of interest.

Acknowledgments

This study was sponsored by the National Natural Science Foundation of China (grant no. 51609071), Fundamental Research Funds for the Central Universities (grant no. 2018B13714), the China Scholarship Council (no. 201806715014), and Science and Technology Project of Guangdong Provincial Communications Department of China (2015-02-013).

References

[1] X. Liu, K. Sheng, Z.-l. Li, L.-q. Gan, H. Shan, and B.-n. Hong, "Experimental Research on foamed mixture lightweight soil mixed with fly-ash and quicklime as backfill material behind abutments of expressway bridge," *Advances in Materials Science and Engineering*, vol. 2017, pp. 1–11, 2017.

[2] X. Tan, W. Chen, H. Tian, and J. Yuan, "Degradation characteristics of foamed concrete with lightweight aggregate and polypropylene fibre under freeze-thaw cycles," *Magazine of Concrete Research*, vol. 65, no. 12, pp. 720–730, 2013.

[3] ASTM, *Standard Test Methods for In-Place Density and Water Content of Soil and Soil-Aggregate by Nuclear Methods (Shallow Depth). ASTM D6938-17a*, ASTM International, West Conshohocken, PA, USA, 2017.

[4] ASTM, *Standard Test Method for Deflections with a Falling-Weight-Type Impulse Load Device, ASTM D4694-09(2015)*, ASTM International, West Conshohocken, PA, USA, 2015.

[5] E. L. Hajduk, M. R. Tallent, D. L. Ledford, and W. R. Christopher, "Crosshole sonic logging integrity testing for the new cooper river bridge," *International Conference on Case Histories in Geotechnical Engineering*, 2004.

[6] BS, *Testing Concrete. Determination of Ultrasonic Pulse Velocity, BS 12504-4*, British Standards Institution, London, UK, 2004.

[7] ASTM, *Standard Test Method for Pulse Velocity Through Concrete*, ASTM C597-16, West Conshohocken, PA, USA, 2016.

[8] DIN, *Testing Concrete in Structures-Part 4: Determination of Ultrasonic Pulse Velocity; German Version, DIN EN 12504-4: 2004-12, Berlin*, 2004.

[9] GOST, *Concrete. Ultrasonic Method of Strength Determination, Russian Version, GOST 17624-2012, Moscow*, 2014.

[10] CECS, *Technical Specification for Testing Concrete Strength by Ultrasonic Rebound Comprehensive Method; Chinese Version, CECS 02:2005*, CECS/TC5, Beijing, China, 2005.

[11] D. N. Nwokoye, A. I. W. Sc, and C. Eng, "Assessment of the elastic moduli of cement paste and mortar phases in concrete from pulse velocity tests," *Cement and Concrete Research*, vol. 4, no. 4, pp. 641–655, 1974.

[12] J. Stepisnik, M. Lukac, and I. Kocuvan, "Measurement of cement hydration by ultrasonics," *American Ceramic Society Bulletin*, vol. 60, no. 4, pp. 481–483, 1981.

[13] P. P. Rao, D. L. Sutton, J. D. Childs, and W. C. Cunningham, "An ultrasonic device for nondestructive testing of oilwell cements at elevated temperatures and pressures," *Journal of Petroleum Technology*, vol. 34, no. 11, pp. 2611–2616, 1982.

[14] H. C. Kim and S. S. Yoon, "Ultrasonic measurements during early-stage hydration of ordinary Portland cement," *Journal of Materials Science*, vol. 23, no. 2, pp. 611–616, 1988.

[15] J. Keating, D. J. Hannant, and A. P. Hibbert, "Correlation between cube strength, ultrasonic pulse velocity and volume change for oil well cement slurries," *Cement and Concrete Research*, vol. 19, no. 5, pp. 715–726, 1989.

[16] Z. Lafhaj, M. Goueygou, A. Djerbi, and M. Kaczmarek, "Correlation between porosity, permeability and ultrasonic parameters of mortar with variable water/cement ratio and water content," *Cement and Concrete Research*, vol. 36, no. 4, pp. 625–633, 2006.

[17] K. Tharmaratnam and B. S. Tan, "Attenuation of ultrasonic pulse in cement mortar," *Cement and Concrete Research*, vol. 20, no. 3, pp. 335–345, 1990.

[18] J. A. Bogas, M. G. Gomes, and A. Gomes, "Compressive strength evaluation of structural lightweight concrete by non-destructive ultrasonic pulse velocity method," *Ultrasonics*, vol. 53, no. 5, pp. 962–972, 2013.

[19] K. Qiu, H. Chen, W. Sun, L. Sun, J. Hong, and G. Zhao, "Determination of mechanical properties of cement asphalt mortar via UPV method," *Journal of Materials in Civil Engineering*, vol. 26, no. 6, article 04014009, 2014.

[20] S. K. Rao, P. Sravana, and T. C. Rao, "Experimental studies in Ultrasonic Pulse Velocity of roller compacted concrete pavement containing fly ash and M-sand," *International Journal of Pavement Research and Technology*, vol. 9, no. 4, pp. 289–301, 2016.

[21] M. Davraz, Ş. Kilinçarslan, M. Koru, and F. Tuzlak, "Investigation of relationships between ultrasonic pulse velocity and thermal conductivity coefficient in foam concretes," *Acta Physica Polonica A*, vol. 130, no. 1, pp. 469-470, 2016.

[22] S. Wei, Z. Yunsheng, and M. R. Jones, "Using the ultrasonic wave transmission method to study the setting behavior of foamed concrete," *Construction and Building Materials*, vol. 51, pp. 62–74, 2014.

[23] A. M. Alexander, "Accuracy of predicting in-situ compressive strength of deteriorated concrete seawall by ndt methods," in *Proceedings of Nondestructive Evaluation of Civil Structures and Materials*, pp. 67–82, Federal Highway Administration and National Science Foundation, Boulder, CO, USA, May 1992.

[24] CECS, *Technical Specification for Cast-In-Situ Foamed Lightweight Soil, CECS249-2008*, China Association for Engineering Construction Standardization, Beijing, China, 2008.

[25] CJJ, *Technical Specification for Foamed Mixture Lightweight Soil Filling Engineering, CJJ/T177*, Ministry of Housing and Urban-Rural Construction of the People's Republic of China, Beijing, China, 2012.

[26] P. Turgut, "Research into the correlation between concrete strength and UPV values," *NDT.net*, vol. 12, no. 12, pp. 1–9, 2004.

[27] F. Niu and X. Zhang, "Research and technical notes acoustic properties of rigid closed-cell plastic foams," *Chinese Journal of Acoustics*, vol. 1, p. 11, 1982.

[28] K. Gunasekaran, R. Annadurai, and P. S. Kumar, "Long term study on compressive and bond strength of coconut shell aggregate concrete," *Construction and Building Materials*, vol. 28, no. 1, pp. 208–215, 2012.

[29] A. E. Brown, *Rationale and Summary of Methods for Determining Ultrasonic Properties of Materials at Lawrence Livermore National Laboratory*, Lawrence Livermore National Lab, Livermore, CA, USA, 1995.

[30] C. Jones, *Hydrocarbons-Physical Properties and Their Relevance to Utilisation*, BookBoon, London, UK, 2010.

[31] E. R. Crain, "Crain's petrophysical handbook, cement integrity logs-part 3—USB/CBIL," https://spec2000.net/07-cementlog3.htm, 2018.

[32] R. Long, *Improvement of Ultrasonic Apparatus for the Routine Inspection of Concrete*, University of London, London, UK, 2000.

[33] R. Jones and I. Fąçąoaru, "Recommendations for testing concrete by the ultrasonic pulse method," *Matériaux et Constructions*, vol. 2, no. 4, pp. 275–284, 1969.

[34] O. V. Antonio and M. E. Flores, "Ultrasonic wave attenuation as a parameter for concrete strength prediction," in *Proceedings of the 25th ASNT Research Symposium*, pp. 23–27, New Orleans LA, USA, April 2016.

[35] J. O. Owino and L. J. Jacobs, "Attenuation measurements in cement-based materials using laser ultrasonics," *Journal of Engineering Mechanics*, vol. 125, no. 6, pp. 637–647, 1999.

[36] I. O. Yaman, Z. Akbay, and H. Aktan, "Numerical modelling and finite element analysis of stress wave propagation for ultrasonic pulse velocity testing of concrete," *Computers and Concrete*, vol. 3, no. 6, pp. 423–437, 2006.

[37] M. D. Banadaki and B. Mohanty, "Numerical simulation of stress wave induced fractures in rock," *International Journal of Impact Engineering*, vol. 40-41, pp. 16–25, 2012.

[38] J. H. Kim and H. G. Kwak, "Nondestructive evaluation of elastic properties of concrete using simulation of surface waves," *Computer-aided Civil & Infrastructure Engineering*, vol. 23, no. 8, pp. 611–624, 2010.

[39] J.-H. Woo, J.-T. Kim, H.-M. Cho, and W.-B. Na, "Finite element simulation of elastic wave propagation in a concrete plate-modeling and damage detection," *Journal of Ocean Engineering and Technology*, vol. 21, no. 6, pp. 26–33, 2007.

[40] Y. S. Cho and S. U. Hong, "The ANN simulation of stress wave based NDT on concrete structures," in *Proceedings of the 7th WSEAS International Conference on System Science and Simulation in Engineering*, pp. 140–146, World Scientific and Engineering Academy and Society (WSEAS), Venice, Italy, November2008.

[41] S. Muralidhara, B. K. R. Prasad, H. Eskandari, and B. L. Karihaloo, "Fracture process zone size and true fracture energy of concrete using acoustic emission," *Construction and Building Materials*, vol. 24, no. 4, pp. 479–486, 2010.

[42] Dassault, "Getting started with abaqus: keywords edition, 3.4 Example: stress wave propagation in a bar," https://classes.engineering.wustl.edu/2009/spring/mase5513/abaqus/docs/v6.5/books/gsx/default.htm?startat=ch03s04.html, 2005.

[43] R. A. Roberts, "Computational prediction of micro-crack induced ultrasound attenuation in CFRP composites," *Journal of Nondestructive Evaluation*, vol. 33, no. 3, pp. 443–457, 2014.

[44] ACI, *Building Code Requirements for Structural Concrete, ACI-318*, American Concrete Institute, Indianapolis, IN, USA, 2014.